Hindawi
Advances in Materials Science and Engineering
Volume 2021, Article ID 1442506, 13 pages
https://doi.org/10.1155/2021/1442506

Research Article

Effect of Sodium Benzenesulfonate on SO_4^{2-} Removal from Water by Polypyrrole-Modified Activated Carbon

Feng Zhang, Dong-Sheng Wang, Fan Yang, Tian-Yu Li, Hong-Yan Li, and Jian-Guo Cui

College of Environmental Science and Engineering, Taiyuan University of Technology, Jinzhong, Shanxi 030600, China

Correspondence should be addressed to Feng Zhang; anuozhang@gmail.com and Jian-Guo Cui; afh2005@163.com

Received 5 July 2021; Revised 13 August 2021; Accepted 8 September 2021; Published 24 September 2021

Academic Editor: Santiago Aparicio

Sodium benzenesulfonate was doped into polypyrrole-modified granular activated carbon (pyrrole-$FeCl_3$·($6H_2O$)-sodium benzenesulfonate-granular activated carbon; PFB-GAC) with the goal of improving the modified GAC's ability to adsorb sulfate from aqueous solutions. At a GAC dosage of 2.5 g and a pyrrole concentration of 1 mol L^{-1}, the adsorption capacity of PFB-GAC prepared using a pyrrole:$FeCl_3$·($6H_2O$):sodium benzenesulfonate ratio of 1000 : 1500 : 1 reached 23.05 mg g^{-1}, which was eight times higher than that for GAC and two times higher than that for polypyrrole-modified GAC without sodium benzenesulfonate. Adsorption was favored under acidic conditions and high initial sulfate concentrations. Doping with sodium benzenesulfonate facilitated polymerization to give polypyrrole. Sodium benzenesulfonate introduced more imino groups to the polypyrrole coating, and the N^+ sites improved ion exchange of Cl^- and SO_4^{2-} and increased the adsorption capacity of sulfate. Adsorption to the PFB-GAC followed pseudo-second-order kinetics. The adsorption isotherm conformed to the Langmuir model, and adsorption was exothermic. Regeneration using a weak alkali (NH_3·H_2O), which released OH^- slowly, caused less damage to the polypyrrole than using a strong alkali (NaOH) as the regeneration reagent. NH_3·H_2O at a concentration of 12 mol L^{-1} (with the same OH^- concentration as 2 mol L^{-1} NaOH) released 85% of the sorbed sulfate in the first adsorption-desorption cycle, and the adsorption capacity remained >6 mg g^{-1}after five adsorption-desorption cycles.

1. Introduction

The sulfate anion is ubiquitous in water. The main sources of SO_4^{2-} to water are dissolution of sulfur-containing minerals and atmospheric precipitation [1]. SO_4^{2-} is not toxic to humans, but drinking water with a high sulfate concentration can cause diarrhea [2], and SO_4^{2-} at a high concentration causes chronic toxic effects in freshwater organisms [3]. The highly concentrated SO_4^{2-} that enters a water environment through discharge will diffuse to the sedimentary layer at the bottom of the body of water. The anaerobic environment in the sediment is favorable for sulfate-reducing bacteria to convert SO_4^{2-} into S^{2-} or H_2S gas [4]. The S^{2-} produced in this reaction can combine with various metal ions to trigger metal sulfide precipitation, which reduces the concentrations of trace elements that are necessary for aquatic plants and disrupts the ecological balance of the water environment [5]. The H_2S generated during this process is also highly toxic, and its presence can cause fish and other aquatic animals to die out in the location, thus ultimately leading the body of water to lose its original ecological function [6]. It is, therefore, extremely important to remove SO_4^{2-} from wastewater.

Currently available methods for removing anions from water include precipitation, adsorption, ion exchange, electrode ionization, membrane treatments, and biological treatments [7, 8]. Reverse osmosis membrane technology stands out among these strategies, because it can effectively separate SO_4^{2-} from water; however, the associated equipment investment is relatively high; the biological methods often require the addition of a carbon source to support the efficient performance of sulfate-reducing bacteria [9]. The adsorption method has attracted the attention of researchers because of its low cost and ease of use. Many novel adsorption materials, such as silicate materials [10], montmorillonite [11], and biosorbent [12], have been developed to separate pollutants from water. Based on the practical engineering applications, activated carbon is still the most

common sorbent that is used. Modifying activated carbon with an ammonium salt, a surfactant, or quaternary ammonium increases the number of positive charges on the surfaces and strongly improves the efficiency of adsorption of negatively charged anions from water [10]. However, some (3%–10%) of the nitrogen-containing chemicals that are used to modify activated carbon can leach from the activated carbon during a water treatment process and cause secondary pollution of the aquatic system receiving the treated water [13]. Polypyrrole (PPy), which is a well-known conductive polymer, has been used to modify activated carbon in recent years, to improve the adsorption capacity of the carbon through its ion exchange properties and to prevent secondary pollution [14–16].

A conductive polymer is a kind of polymer material formed by chemically or electrochemically doping a polymer with conjugated π-bonds [17]. PPy, which has positively charged nitrogen atoms, can be formed by oxidizing and polymerizing pyrrole (Py) monomers using $FeCl_3{\cdot}(6H_2O)$. The PPy structure is conjugated and has alternating C–C and C=C bonds. Chloride ions (Cl^-) incorporated during the oxidation-polymerization process allow PPy to act as an ion exchange material [7, 18, 19]. PPy has been directly polymerized on activated carbon surfaces to effectively remove anions from water [8, 20]. PPy has mainly been used to treat water to remove NO_3^- [21, 22], F^- [23, 24], and SO_4^{2-} [9, 25].

Polymerization of Py can equally occur at the α and β positions, so PPy grows in three dimensions during polymerization [26, 27]. Three-dimensional growth of PPy will give relatively few planarization defects [24], meaning the PPy will readily be attacked by OH^- (a strong nucleophile) once Cl^- is incorporated, and deprotonation has occurred [26]. The presence of planar aromatic benzene sulfonate (e.g., sodium benzenesulfonate (BSNa)) anions during polymerization could limit three-dimensional growth of PPy and therefore promote an orderly arrangement of PPy chains, which would cause the PPy to grow in a laminar fashion and have a dense and ordered surface morphology [26, 27]. Preparing PPy using this doping method should give PPy-modified activated carbon with a better anion exchange performance than PPy-modified activated carbon produced without doping. However, using doping anions that are too large (e.g., sodium dodecylbenzenesulfonate) will give PPy chains separated so much that interchain jumping by the carriers is hindered, and ion exchange cannot occur [28–30].

The ions in a PPy film will form galvanic cells on the surfaces because of the difference in the oxygen concentrations at the surface and in the bulk solution [31]. Hydroxide ions in the solution could attack the imino groups in PPy to form carbonyl groups, which will gradually decrease the ion exchange capacity of the PPy [27]. Doping with BSNa will increase the ion gap in the PPy and prevent galvanic cells forming.

In addition to efficient adsorption, efficient desorption and regeneration are extremely important when developing an adsorption material. OH^- strongly attacks PPy and can remove the doped ions [26], so strong alkalis such as sodium hydroxide are often used to regenerate PPy. Bhaumik et al. [23] found that 97% of the F^- ions adsorbed by a PPy/Fe_3O_4 nanomagnetic material desorbed by increasing the pH to 12. Pahlavanzadeh et al. [32] used 0.1–1 M NaOH to desorb NO_3^- adsorbed to PPy/sawdust and found PPy/sawdust regeneration rates of between 10% and 35% at different NaOH concentrations. Hydroxyl anions and imino groups will react rapidly in a strong alkaline environment, meaning that PPy will be damaged [27], so ammonium hydroxide ($NH_3{\cdot}H_2O$), which is a weak alkaline, has also been used as a PPy regenerating agent.

In this study, a method involving doping with BSNa was used to produce granular activated carbon (GAC) modified with PPy (PFB-GAC). The effects of the PFB-GAC preparation conditions and reaction conditions on SO_4^{2-} adsorption were investigated. The PFB-GAC was characterized by scanning electron microscopy (SEM), Brunauer–Emmett–Teller (BET) surface area analysis, energy-dispersive X-ray spectroscopy (EDS), and Fourier-transform infrared spectroscopy to investigate the mechanism through which the PFB-GAC adsorbed SO_4^{2-}. The PFB-GAC performance was assessed using adsorption kinetic, adsorption isotherm, and adsorption thermodynamic data. Adsorption-desorption cycles were performed under alkaline conditions (using $NH_3{\cdot}H_2O$) to assess the recyclability of the PFB-GAC. The results were expected to indicate whether the PFB-GAC could be used to remove SO_4^{2-} from acidic wastewater.

2. Materials and Methods

2.1. Materials. Activated coconut shell carbon for purifying water (20 mesh) was purchased from Hua Jing (Chengde, China). Py (C_4H_5N), iron chloride hexahydrate ($FeCl_3{\cdot}(6H_2O)$), anhydrous sodium sulfate (Na_2SO_4), sodium hydroxide (NaOH), hydrochloric acid (HCl), BSNa ($C_6H_5SO_3Na$), ammonium hydroxide ($NH_3{\cdot}H_2O$), and other chemicals were of analytical grade and were purchased from Aladdin (Shanghai, China). All chemicals were used as received, without further purification, and all solutions were prepared using ultrapure water obtained from a ZMQS5001 system (Milli-Q, USA).

2.2. Adsorbent Synthesis. The PPy-modified GAC doped with BSNa was prepared from pristine GAC that had been ground and wet-sieved to Chinese mesh size 20 (0.9 mm). The GAC was repeatedly washed with ultrapure water and then dried at 328 K in a vacuum drying oven for 24 h to a constant weight. A 2.5 g aliquot of the dry GAC was added to a glass bottle, and then 50 mL of Py that had been distilled using a rotary evaporator and had a specified molar concentration was added to the bottle. The bottle was sealed and placed in a thermostat-controlled oscillator and then oscillated at 180 revolutions min^{-1} for 12 h at 298 K. The supernatant was discarded, then 50 mL of FeCl3·(6H2O) at a specified molar concentration was added, and the bottle was oscillated for 5 h. Then, a specified molar concentration of BSNa was added, and the bottle was oscillated for 3 h. The PFB-GAC was then

collected by passing the mixture through a funnel containing filter paper. The PFB-GAC was rinsed three times each with deionized water, anhydrous ethanol, and deionized water, in that order, and then dried in a vacuum drying oven. The PFB-GAC was dried for 24 h at 328 K. Unused PFB-GAC was stored in a nitrogen atmosphere at a low temperature in the dark.

The improvement in SO_4^{2-} adsorption by PFB-GAC relative to other adsorbents was investigated by performing experiments using GAC modified separately with FeCl3·(6H2O), BSNa, and Py and with GAC modified with FeCl3·(6H2O) plus BSNa, GAC modified with Py plus FeCl3·(6H2O) (PF-GAC), and GAC modified with Py plus BSNa.

2.3. Batch Adsorption. Adsorption experiments were performed to investigate the effects of different conditions on SO_4^{2-} adsorption and to identify the conditions that caused the largest amount of SO_4^{2-} to be removed. Each adsorption experiment was performed using 50 mL of a 500 mg L−1 SO_4^{2-} solution at neutral pH in a conical flask kept at 298 ± 1 K in a constant-temperature oscillator set to oscillate at 180 revolutions min−1. Different parameters were used in different experiments. The effects of using different initial SO_4^{2-} concentrations, pH values, and initial temperatures on the adsorption capacity at equilibrium were studied, and the adsorption kinetics and adsorption isotherms were investigated. The adsorbent dose m_s was always 0.2 g except when tests were performed to investigate the effect of using different adsorbent doses. The pH was adjusted by adding 0.1 mol L^{-1} NaOH or HCl. The ion chromatography column was protected from organic matter by passing each supernatant sample through a C_{18} cartridge and a 0.22 μm filter before the SO_4^{2-} concentration was determined. It was found in preliminary experiments that the sample pretreatment did not affect the SO_4^{2-} concentration. Each test was performed in duplicate, and the mean concentration is presented.

The adsorption capacity at equilibrium q_e (mg g^{-1}) was calculated using the following equation [33]:

$$q_e = \frac{(C_0 - C_e)V}{m_s}. \quad (1)$$

The adsorption capacity q_t (mg g^{-1}) at contact time t (min) was calculated using the following equation:

$$q_t = \frac{(C_0 - C_t)V}{m_s}. \quad (2)$$

The mass m_{ads} (mg) of adsorbed SO_4^{2-} was calculated using the following equation:

$$m_{a\,ds} = m_s \times q_e, \quad (3)$$

here, C_0, C_e, and C_t are the initial adsorbate concentration (mg L^{-1}), adsorbate concentration (mg L^{-1}) at equilibrium, and adsorbate concentration (mg L^{-1}) at time t (min), respectively, V is the volume of the solution (mL), and m_s (g) is the dry weight of adsorbent.

2.4. Desorption Experiments. A saturated PFB-GAC sample was transferred to a 10 mL bottle, and a specified concentration of the regeneration solution was added. The bottle was sealed and shaken for a specified time, and then the supernatant was analyzed to determine the concentration of SO_4^{2-} that had been desorbed from the PFB-GAC. The desorption and regeneration time was 40 min, the temperature was 298 K, and the regeneration solution volume was 1 mL. After desorption, the PFB-GAC was removed from the mixture by filtering the mixture, and then the PFB-GAC was washed with deionized water and dried in a vacuum oven. A fresh aliquot of SO_4^{2-} solution was then added before the desorption process was repeated.

The mass of desorbed SO_4^{2-} m_i (mg) was calculated using the following equation:

$$m_i = C_i \times V, \quad (4)$$

where C_i is the SO_4^{2-} concentration (mg L^{-1}) in the desorption solution and V is the volume of the regeneration solution. The desorption efficiency D (%) was calculated using the following equation:

$$D(\%) = \frac{m_i}{m_{a\,ds}} \times 100\%. \quad (5)$$

2.5. Analytical Methods. The SO_4^{2-} concentration was determined using a CIC-D120 ion chromatograph (ShengHan, Qingdao, China) equipped with a polystyrene-divinylbenzene column (250 mm long, 4.0 mm i.d.). The anion eluent contained sodium carbonate and sodium bicarbonate at a molar ratio of 1 : 1.

The surface structure and element composition of the adsorbent were investigated by SEM and EDS using a JSM-7100F instrument (JEOL, Tokyo, Japan) at magnifications of 2000 and 7000. The surface area and porosity of the adsorbent were investigated by performing BET analysis using MicroActive software for ASAP2460 system (Micromeritics, Norcross, GA, USA) at 418 K using N_2. Fourier-transform infrared spectroscopy was performed using a TENSOR 27 system (Bruker, Billerica, MA, USA) to identify changes in functional groups during the PFB-GAC preparation procedure and through adsorption of SO_4^{2-}.

3. Results and Discussion

3.1. Influences of the PFB-GAC Preparation Conditions

3.1.1. Effects of Using Different Py and $FeCl_3$·($6H_2O$) Ratios on SO_4^{2-} Adsorption. Modified GAC was prepared from 2.5 g of GAC and Py at a concentration of 1 mol L^{-1}. A 0.2 g aliquot of modified GAC was added to each of a series of conical flasks, and then 50 mL of 500 mg L^{-1} Na_2SO_4 was added to each flask.

It can be seen from Figure S1 that the adsorption capacity of the PF-GAC reached 11 mg g^{-1}, which was about five times higher than the adsorption capacity of the GAC. However, the adsorption capacities were lower for the Py-BSNa-GAC and $FeCl_3$·($6H_2O$)-BSNa-GAC than for the

GAC. This indicated that oxidation of Py because of the $FeCl_3{\cdot}(6H_2O)$ doping and polymerization to give PPy caused ion exchange to occur, as has been found in previous studies [7, 18, 19].

The effect of the Py : $FeCl_3{\cdot}(6H_2O)$ (P : F) ratio on SO_4^{2-} adsorption by the PF-GAC was investigated, and the SO_4^{2-} adsorption capacity results are shown in Figure 1. It can be seen that the amount of SO_4^{2-}adsorbed gradually increased as the amount of Py used increased. At a P : F ratio of 1 : 1.5, the adsorption capacity was about seven times higher than the adsorption capacity of the GAC. The results indicated that the adsorption rate could still be increased when the P : F ratio was increased to more than 5 : 1. However, the cost of preparing the modified adsorbent led to subsequent PFB-GAC tests being performed using P : F ratios between 1 : 1 and 1 : 3.

3.1.2. Effect of the BSNa Concentration on SO_4^{2-} Adsorption by the Modified GAC. Modified GAC was prepared using different BSNa concentrations (1, 0.1, 0.01, 0.001, and 0.0001 mol L^{-1}) and P : F ratios (1 : 1.5 and 1 : 3).

The adsorption capacity was determined after performing static 25 min adsorption tests at 298 K. The results are shown in Figure 2. SO_4^{2-} was adsorbed more effectively by the modified GAC prepared using a P : F ratio of 1 : 1.5 and a BSNa concentration of 10^{-3} mol L^{-1} than by the other modified GAC samples. At the same BSNa concentration, SO_4^{2-} was adsorbed more effectively when the P : F ratio was 1 : 1.5 than when the P : F ratio was 1 : 3.

The amount of SO_4^{2-} adsorbed by the modified GAC gradually increased as the BSNa dose increased. The adsorption capacity decreased when the BSNa dose increased above 10^{-3} mol L^{-1}. For the same amount of PPy, increasing the BSNa dose may decrease ion exchange between SO_4^{2-} and Cl^-.

3.2. PFB-GAC Performance

3.2.1. Adsorption of SO_4^{2-} by the PFB-GAC at Different Initial SO_4^{2-} Concentrations. Modified GAC was prepared using a Py : $FeCl_3{\cdot}(6H_2O)$: BSNa (P : F : B) molar ratio of 1000 : 1500 : 1. Adsorption of SO_4^{2-} by this modified GAC was assessed, and adsorption of SO_4^{2-} by PF-GAC and GAC was also assessed for comparison. The three types of GAC described above were used to adsorb SO_4^{2-} from solutions with different initial SO_4^{2-} concentrations (400, 500, 600, 700, and 800 mg L^{-1}), and the results are shown in Figure 3.

The SO_4^{2-} adsorption capacity of the PFB-GAC prepared using a P : F : B ratio of 1000 : 1500 : 1 was almost double the SO_4^{2-} adsorption capacity of the PF-GAC prepared using a P : F ratio of 1 : 1.5 and about eight times higher than the SO_4^{2-} adsorption capacity of the GAC. The amount of SO_4^{2-} adsorbed by the PFB-GAC gradually increased as the initial SO_4^{2-} concentration increased. When the initial SO_4^{2-} concentration was 800 mg L^{-1}, the adsorption capacity of the PFB-GAC was 20.23 mg g^{-1}, which was 1.3 times higher than the adsorption capacity of 15.49 mg g^{-1} found when the initial SO_4^{2-} concentration was 300 mg L^{-1}. Assuming that the number of adsorption sites was constant, the results indicate that increasing the SO_4^{2-} concentration difference at the adsorption interface may promote diffusion of SO_4^{2-} to the adsorption material surfaces.

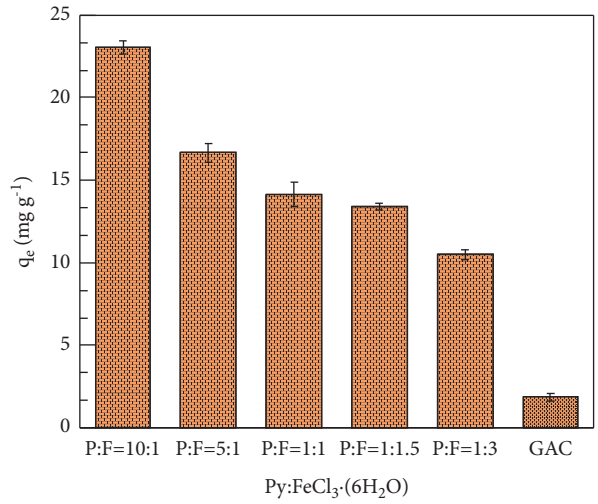

Figure 1: Effect of the pyrrole (Py) and $FeCl_3{\cdot}(6H_2O)$ molar ratio (P : F) on SO_4^{2-} adsorption (GAC = granular activated carbon).

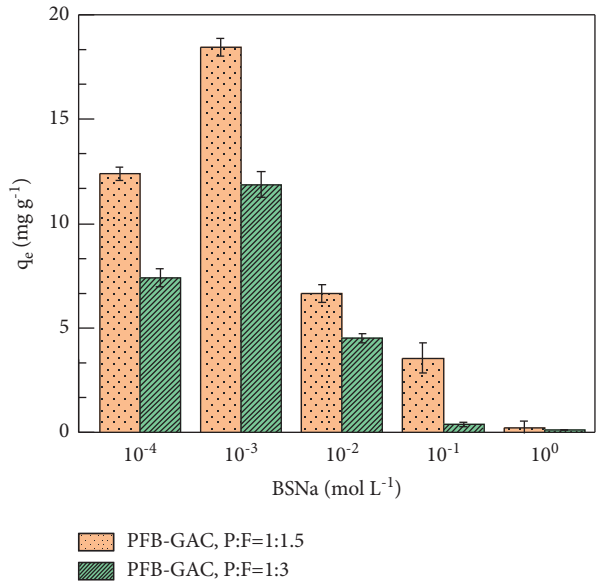

Figure 2: Effects of the pyrrole:$FeCl_3{\cdot}(6H_2O)$ molar ratio (P : F) and sodium benzenesulfonate (BSNa) concentration on SO_4^{2-} adsorption (PFB-GAC = pyrrole-$FeCl_3{\cdot}(6H_2O)$-BSNa-granular activated carbon).

3.2.2. Effect of pH on SO_4^{2-} Removal. The effect of the pH on SO_4^{2-} adsorption was studied using a PFB-GAC dose of 4 g L^{-1}, an initial SO_4^{2-} concentration of 500 mg L^{-1}, and pH values between 2.0 and 12.0. The results are shown in Figure 4. It can be seen that the PFB-GAC most effectively adsorbed SO_4^{2-} when the initial pH was 2.0. Between pH 3.0 and 5.0, the adsorption capacity decreased slightly as the pH increased. Increasing the pH further favored exchange

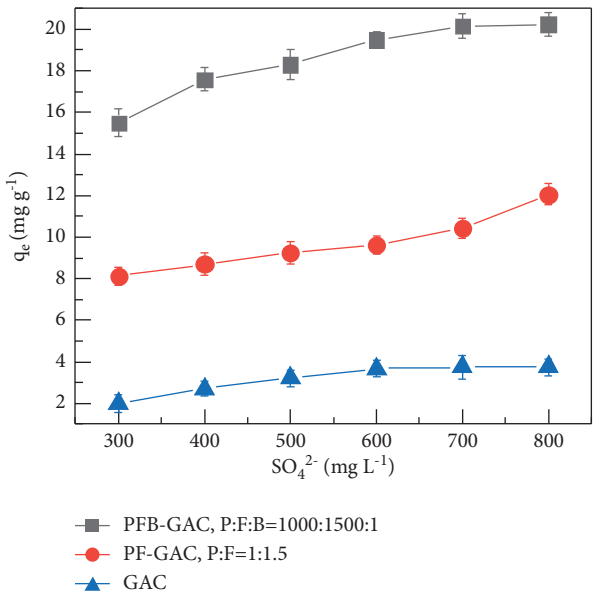

FIGURE 3: SO_4^{2-} adsorption capacities at equilibrium when different initial SO_4^{2-} concentrations were used (PFB-GAC = pyrrole-$FeCl_3$·($6H_2O$)-sodium benzenesulfonate-granular activated carbon, P : F : B = pyrrole:$FeCl_3$·($6H_2O$):sodium benzenesulfonate molar ratio, PF-GAC = pyrrole-$FeCl_3$·($6H_2O$)-granular activated carbon, P : F = pyrrole:$FeCl_3$·($6H_2O$) molar ratio, and GAC = -granular activated carbon).

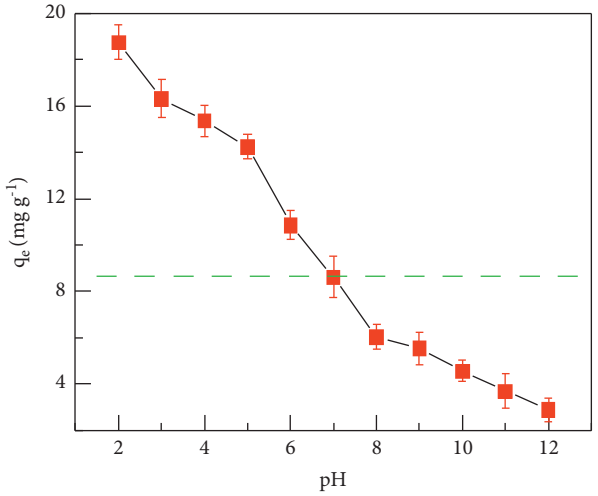

FIGURE 4: SO_4^{2-} adsorption by pyrrole-$FeCl_3$·($6H_2O$)-sodium benzenesulfonate-granular activated carbon at different initial pH values.

between OH^- and SO_4^{2-} that had been adsorbed by the PFB-GAC, resulting in SO_4^{2-} desorption, because of the high OH^- concentration especially under alkaline conditions. Münstedt [34] investigated the electrical conductivity of the PPy film treated with base or acid and found that its conductivity was markedly reduced following a strong alkali treatment, whereas it remained essentially unchanged under highly acidic conditions. Generally, PPy film is more stable in acidic environment [35], which might be the reason why it exhibited higher anion adsorption efficiency. The hydroxide ions can attack imino groups and damage the PPy, and deprotonation could also occur [24, 26].

3.2.3. Effect of Temperature on SO_4^{2-} Removal. The effects of the temperature on SO_4^{2-} adsorption by the PFB-GAC when the adsorbent dose was 4 g L^{-1} are shown in Figure 5. It can be seen that the SO_4^{2-} adsorption capacity of the PFB-GAC gradually increased as the temperature decreased whatever the initial SO_4^{2-}concentration is. This indicated that the adsorption process was exothermic and that decreasing the temperature promoted SO_4^{2-} adsorption by the PFB-GAC.

3.3. Characterization of the PFB-GAC

3.3.1. SEM Analysis. The SEM results are shown in Figure 6. Images A_1 and A_2 are SEM images of the unmodified GAC. It can be seen that the GAC had abundant evenly distributed pores on the surfaces, making it a good carrier for PPy. Images B_1 and B_2 are SEM images of the PPy-modified GAC. It can be seen when comparing images A_1 and A_2 with images B_1 and B_2 that PF had been successfully loaded onto the PF-GAC. The pores on the GAC surfaces became fewer and smaller because of PPy being loaded onto the pore surfaces, partly blocking the pores [36].

Images C_1 and C_2 are SEM images of the oxidized polymerized PPy doped with BSNa. Some bulky substances were added to the surfaces. The BSNa played a role in the PPy polymerization process and caused the coating to be more continuous than the coating of the GAC coated only with PPy [37]. The BSNa connected PPy strands together, so it increased the degree of polymerization of the PPy and decreased PPy shedding during the adsorption process.

3.3.2. BET Analysis. The BET analysis results indicated that the BET surface area of the PFB-GAC was 725.2964 m^2 g^{-1}, but the BET surface area of the GAC was 5.9400 m^2 g^{-1}. The adsorption and desorption isotherms and pore size distribution curves of the GAC and PFB-GAC are shown in Figure 7(a) (GAC) and Figure 7(b) (PFB-GAC). According to the International Union of Pure and Applied Chemistry classification, the PFB had a type I adsorption isotherm, but the macroporous GAC had a type II adsorption isotherm. This and the pore size distribution suggest that the PFB coating occupied the large pores in the GAC and that more micropores formed. The PFB coating caused the macroporous GAC to become an adsorbent with well-developed mesopores (pore size <2 nm). The SEM and BET analysis results indicated that the PFB coating adhered well to the large pores and outer surfaces of the GAC and gave the PFB-GAC many micropores.

3.3.3. EDS. As shown in Figure 8, EDS indicated that the N contents of the GAC, PF-GAC, and PFB-GAC were 3%, 10.2%, and 12.8%, respectively. Approximately 25% of the N in PPy would have been N^+ [22], and the nitrogen content of GAC loaded with PPy was markedly higher than the nitrogen content of the GAC. When the same number of moles

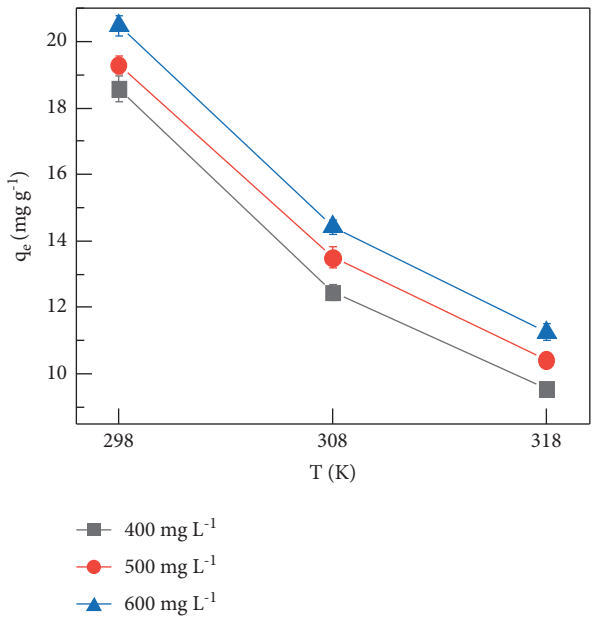

FIGURE 5: Effect of the temperature on SO_4^{2-} adsorption by the pyrrole-$FeCl_3$·($6H_2O$)-sodium benzenesulfonate-granular activated carbon.

of Py was used, the nitrogen content was higher when BSNa was present than when BSNa was not present.

Loading the GAC with PPy increased the amount of N^+ on the surfaces, and the more positively charged sites would have been occupied by Cl^- and would have provided active sites for ion exchange with SO_4^{2-}. Doping with BSNa controlled PPy growth in certain directions and would control and limit spatial growth of the PPy produced through polymerization of Py [37]. The PPy would therefore grow in an orderly manner in a specific direction or in a specific area rather than three-dimensionally. The PPy on the GAC surfaces therefore had a more regular morphology and was more stable when BSNa was present than when BSNa was not present. The BSNa also played a role in causing planes to form in the PPy, and therefore, more PPy to be loaded on the GAC surfaces, which would have increased the conductivity and ion exchange capacity of the PPy.

The imino group in PPy can, to some extent, act as a reducing agent [38], but SO_4^{2-} is relatively stable. The ability of PPy to act as a reducing agent would therefore have decreased the SO_4^{2-} concentration in the water little.

3.3.4. Fourier-Transform Infrared Spectroscopy. The Fourier-transform infrared spectra of the GAC, PFB-GAC, and PFB-GAC with adsorbed SO_4^{2-} are shown in Figures 9(a)–9(c), respectively. The PFB-GAC surfaces were found to have abundant functional groups. There was a strong wide absorption band at 3430 cm^{-1}, which was assigned to intermolecular hydrogen bonds and overlapping bands for O–H and N–H stretching vibrations. The main PPy bands were at 1543 cm^{-1} (C–C stretching vibrations in the pyrrole ring) and 1450 cm^{-1} (stretching vibrations of C–N in the ring), and there was a local absorption maximum at 1164 cm^{-1} (symmetric stretching vibration of the pyrrole ring). A band at 1039 cm^{-1} was assigned to deformation vibrations in the C–H and N–H planes of the pyrrole ring, and the lowest value of the spectrum corresponded to deformation vibrations outside the C–H plane of the ring [39]. PPy was successfully anchored to the GAC, and loading PPy onto the GAC clearly changed the functional groups attached to the GAC. There was a particularly large change at around 3430 cm^{-1}, which was assigned to N–H groups and clearly indicated that the amount of N^+ present was increased by the modification process.

3.4. Adsorption Kinetics. The kinetics of SO_4^{2-} adsorption onto the PFB-GAC are shown in Figure 10. The results indicated that the PFB-GAC strongly removed SO_4^{2-} in the first 25 min, and then the amount of SO_4^{2-} adsorbed remained stable. This indicated that the PFB-GAC could be used to quickly adsorb SO_4^{2-}. The pseudo-first-order and pseudo-second-order kinetics models were fitted to the experimental data. The data and lines are shown in Figures S2 and S3, and the fitting parameters are shown in Table 1. The pseudo-second-order kinetics model fitted the data well. The pseudo-first-order kinetics model is related to physical adsorption processes, and the pseudo-second-order kinetics model describes chemical adsorption processes based on electron sharing [39]. The fitting results indicated that the adsorption process included chemical adsorption. The linear forms of the pseudo-first-order and pseudo-second-order kinetics equations are shown in the following equations, respectively.

$$\frac{dq_t}{dt} = k_1 q_e - q_t \Rightarrow \ln q_e - q_t = \ln q_e - \frac{k_1 t}{2.303}, \quad (6)$$

$$\frac{dq_t}{dt} = k_2 (q_e - q_t)^2 \Rightarrow \frac{t}{q_t} = \frac{1}{k_2 q_e^2} + \frac{t}{q_e}. \quad (7)$$

In equations (6) and (7), q_e (mg g^{-1}) and q_t (mg g^{-1}) are the amounts of SO_4^{2-} adsorbed onto the modified GAC at equilibrium and at time t, respectively, and k_1 (min^{-1}) and k_2 (g (min mg)$^{-1}$) are the pseudo-first-order and pseudo-second-order adsorption rate constants, respectively.

3.5. Adsorption Isotherms. For the Langmuir model, it is assumed that adsorption occurs on the adsorbent surface uniformly and that no migration occurs. The Langmuir model is suitable for single-layer adsorption, adsorbents with homogeneous sites on the surfaces, and a uniform energy-level distribution. The Freundlich model is not limited to single-layer adsorption and can be used as an empirical adsorption model for uneven surface conditions.

The Langmuir equation can be rearranged to give a linear form to make it convenient to plot the model and determine the Langmuir constants (k_L), as shown below. The linear form of the Langmuir model is shown in equation (8). The q_m and k_L values can be determined from a linear plot of C_e q_e^{-1} against C_e.

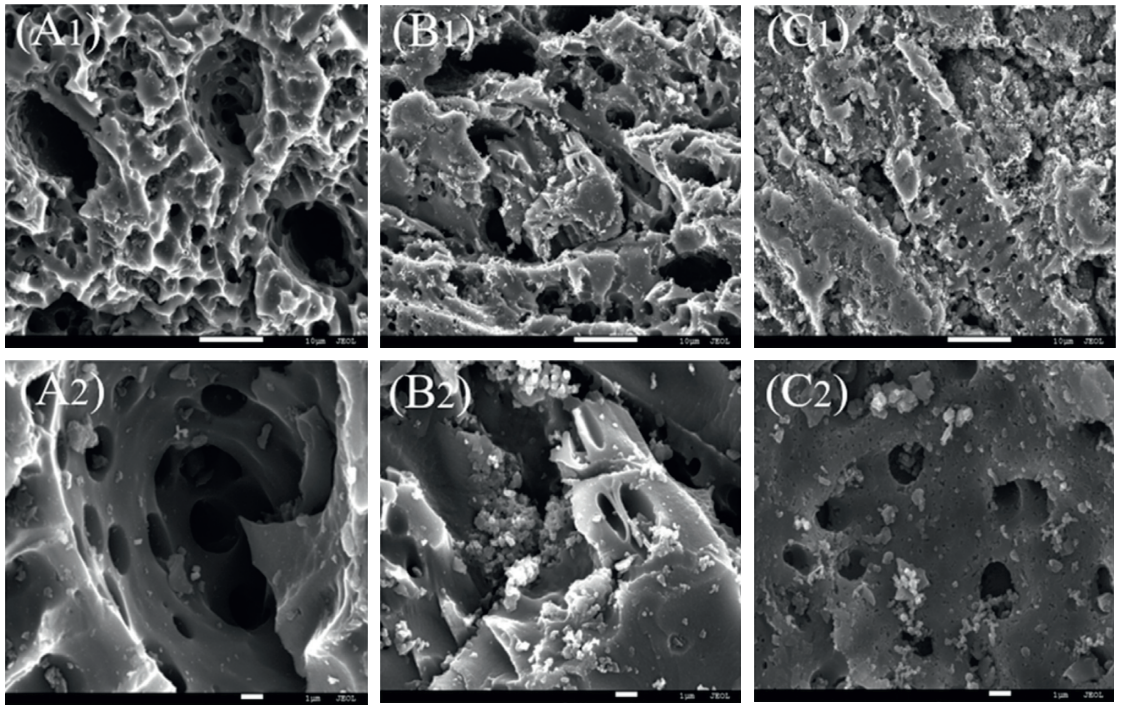

Figure 6: Scanning electron microscopy images of (A_1) granular activated carbon, (B_1) pyrrole-$FeCl_3$·($6H_2O$)-granular activated carbon, and (C_1) pyrrole-$FeCl_3$·($6H_2O$)-sodium benzenesulfonate-granular activated carbon at a magnification of 2000 and of (A_2) granular activated carbon, (B_2) pyrrole-$FeCl_3$·($6H_2O$)-granular activated carbon, and (C_2) pyrrole-$FeCl_3$·($6H_2O$)-sodium benzenesulfonate-granular activated carbon at a magnification of 7000.

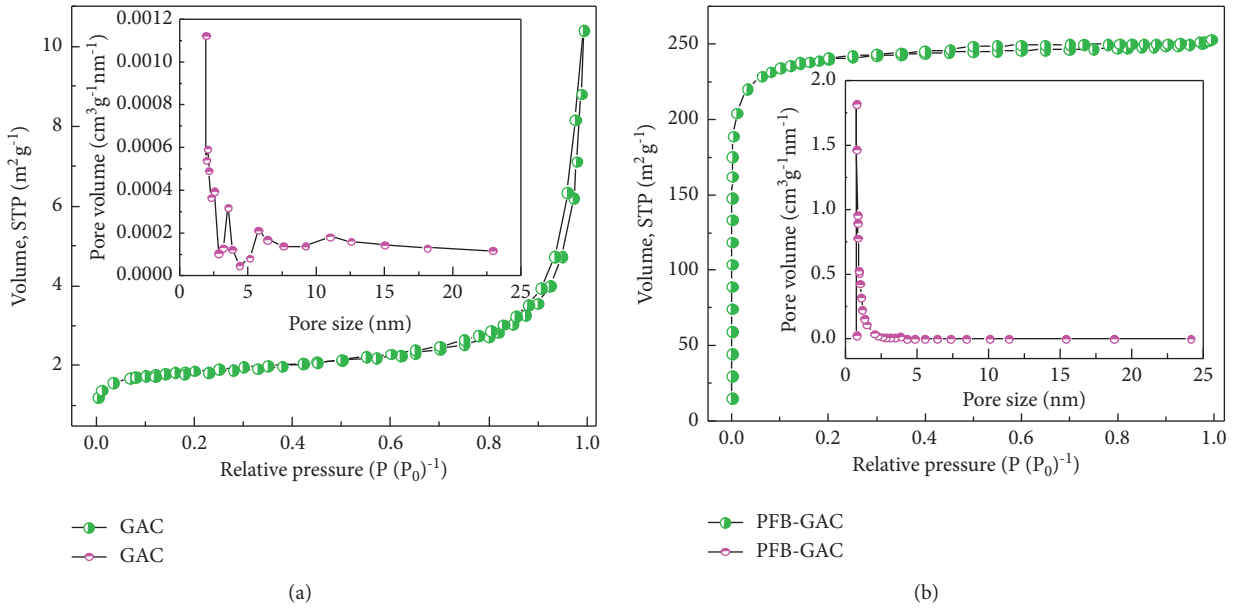

Figure 7: N_2 adsorption and desorption isotherms and pore size distributions for (a) the granular activated carbon (GAC) and (b) the pyrrole-$FeCl_3$·($6H_2O$)-sodium benzenesulfonate-granular activated carbon (PFB-GAC).

$$q_e = \frac{q_m k_L C_e}{1 + k_L C_e} \Rightarrow \frac{C_e}{q_e} = \frac{1}{k_L q_m} + \frac{C_e}{q_m}. \quad (8)$$

In equation (8), Ce is the SO_4^{2-} concentration at equilibrium (mg L^{-1}), q_e is the amount of SO_4^{2-} adsorbed at equilibrium (mg g^{-1}), q_m is the maximum amount of SO_4^{2-} adsorbed (mg g^{-1}), and k_L is a constant (L mg^{-1}).

The Freundlich isotherm equation is based on adsorption onto nonuniform surfaces. The Freundlich isotherm equation is shown in the following equation:

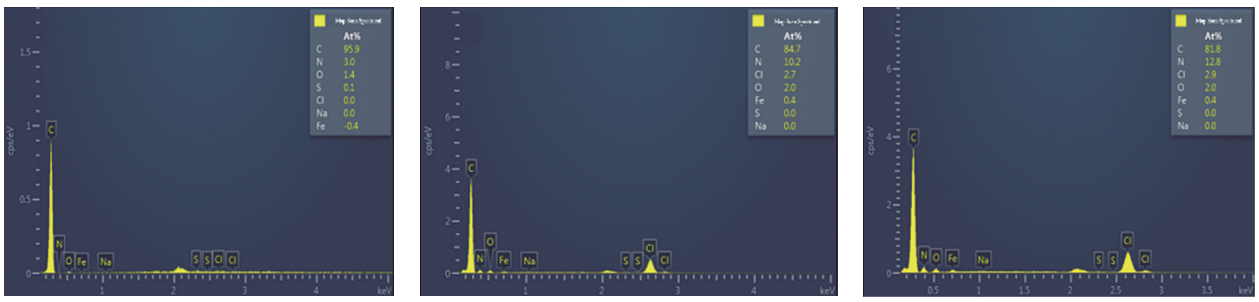

(a) (b) (c)

FIGURE 8: Energy-dispersive X-ray spectra of the (a) granular activated carbon, (b) pyrrole-$FeCl_3$·($6H_2O$)-granular activated carbon, and (c) pyrrole-$FeCl_3$·($6H_2O$)-sodium benzenesulfonate-granular activated carbon.

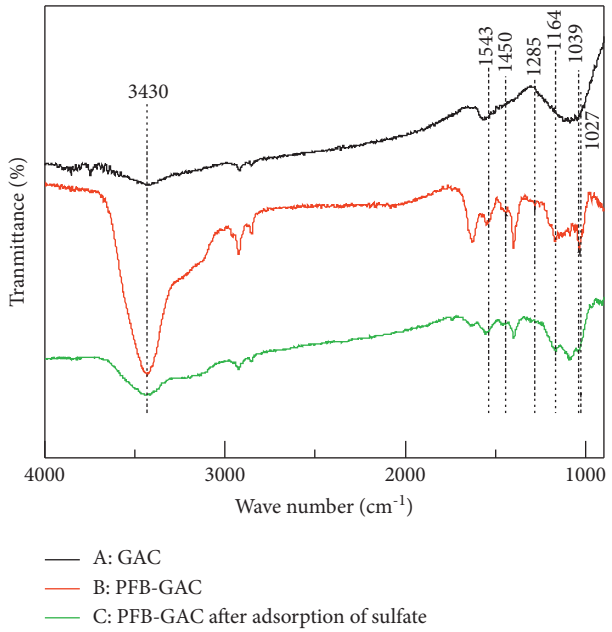

FIGURE 9: Fourier-transform infrared spectra of (a) granular activated carbon (GAC), (b) pyrrole-$FeCl_3$·($6H_2O$)-sodium benzenesulfonate (PFB)-GAC, and (c) PFB-GAC with SO_4^{2-} adsorbed.

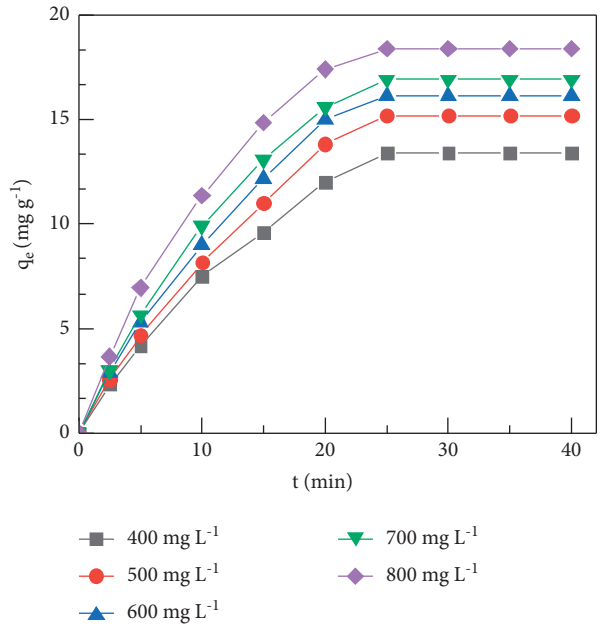

FIGURE 10: Kinetics of SO_4^{2-} adsorption onto pyrrole-$FeCl_3$·($6H_2O$)-sodium benzenesulfonate-granular activated carbon.

$$q_e = k_F + C_e^{1/n} \Rightarrow \ln q_e = \ln k_F + \frac{1}{n} \ln C_e. \quad (9)$$

In equation (9), k_F (mg g^{-1}) is the Freundlich constant related to the adsorption capacity and adsorption strength and $1/n$ is the heterogeneity factor.

The results of the adsorption isotherm experiments are shown in Figure 11, and the calculated parameters for the Langmuir and Freundlich models are shown in Table 2. The Langmuir and Freundlich isotherms are shown in Figures S4 and S5, respectively. The R^2 values for the Langmuir model were 0.9933–0.9977, and the R^2 values for the Freundlich model were 0.9482–0.9956, indicating that SO_4^{2-} adsorption onto the PFB-GAC was described better by the Langmuir model than the Freundlich model. This indicated that the PFB-GAC surfaces adsorbed a single layer of SO_4^{2-}, the adsorption sites were homogeneous, and the energy-level distribution was uniform. The SO_4^{2-} adsorption rate K_L gradually decreased as the reaction temperature increased, indicating that the adsorption process was exothermic. This was consistent with the effect of the temperature on the adsorption capacity discussed in Section 3.2.3.

3.6. Adsorption Thermodynamics. Three thermodynamic parameters, standard enthalpy (ΔH^0), standard free energy (ΔG^0), and standard entropy (ΔS^0), were assessed. The ΔG^0, ΔH^0, and ΔS^0 values were calculated using the following equations:

$$\Delta G^0 = -RT \ln K_C. \quad (10)$$

The relationship between ΔG^0, ΔH^0, and ΔS^0 is described by the following equation:

$$\Delta G^0 = \Delta H^0 - T\Delta S^0. \quad (11)$$

The van 't Hoff equation is

Table 1: Kinetics parameters for SO_4^{2-} adsorption.

C_0 (mg L^{-1})$^{-1}$	Pseudo-first-order model			Pseudo-second-order model		
	k_1 (min^{-1})	q_e (mg g^{-1})	R^2	k_2 (min^{-1})	q_e (mg g^{-1})	R^2
400	0.2684	17.331	0.9418	0.0012	29.239	0.9981
500	0.3298	21.911	0.9033	0.0008	35.842	0.9906
600	0.3315	22.642	0.9282	0.0011	34.483	0.9903
700	0.3196	21.865	0.9622	0.0011	35.587	0.9919
800	0.3094	23.231	0.9729	0.0015	33.670	0.9906

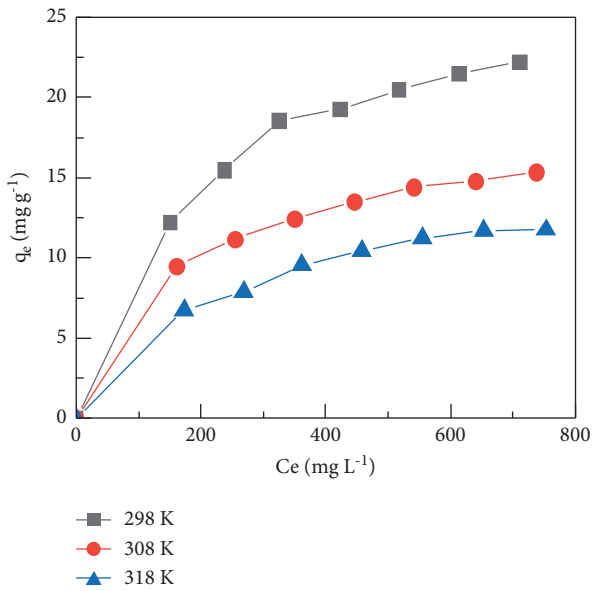

Figure 11: Isotherms for SO_4^{2-} adsorption onto the pyrrole-$FeCl_3$·($6H_2O$)-sodium benzenesulfonate-granular activated carbon.

Table 2: Isotherm parameters for the adsorption of SO_4^{2-} onto the pyrrole-$FeCl_3$·($6H_2O$)-sodium benzenesulfonate-granular activated carbon.

T(K)	Langmuir model			Freundlich model		
	q_m(mg g^{-1})	k_L (L mg^{-1})	R^2	n	k_F (mg g^{-1})	R^2
298	27.7778	0.0053	0.9977	3.8388	4.0257	0.9956
308	19.8413	0.0047	0.9977	2.5107	1.1574	0.9482
318	15.8730	0.0041	0.9933	2.4691	0.8464	0.9743

$$\ln K_C = \frac{\Delta S^0}{R} - \frac{\Delta H^0}{RT}, \quad (12)$$

where R (8.314 J mol^{-1} K) is the universal gas constant, T (K) is the absolute temperature of the solution, and Kc (L mol^{-1}) is the Langmuir constant, which can be determined by identifying the intercept of the line fitted to a plot of C_e q_e^{-1} against C_e.

A plot of lnKc against 1/T is shown in Figure S6. A line was fitted to the plot to allow the van 't Hoff equation parameters to be determined. The enthalpy change was defined as the slope of the line (ΔH^0 R^{-1}), and the entropy change was defined as the intercept of (ΔS^0 R^{-1}). The calculated ΔG^0, ΔH^0, and ΔS^0 values for SO_4^{2-} adsorption onto the PFB-GAC are shown in Table 3. The enthalpy change (ΔH^0) was negative, indicating that lower temperatures favored adsorption, which was consistent with the conclusions drawn from the adsorption isotherms. The entropy change (ΔS^0) was negative, indicating that the PFB-GAC structure was not markedly changed by the adsorption process and that adsorption decreased randomness in the system. The negative ΔG^0 value indicated that adsorption was spontaneous.

Table 3: Thermodynamic parameters for SO_4^{2-} adsorption onto pyrrole-$FeCl_3$·($6H_2O$)-sodium benzenesulfonate-granular activated carbon.

T (K)	ΔG^0 (KJ mol^{-1})	ΔH^0 (KJ mol^{-1})	ΔS^0 (J mol^{-1} K^{-1})
298	−7.587		
308	−7.533	−10.471	−9.633
318	−7.392		

3.7. Desorption and Reuse. Batch desorption experiments were performed using deionized water, sodium hydroxide, and ammonium hydroxide (mass concentration 25%) as desorbents. When deionized water was used, <3% of the adsorbed SO_4^{2-} was desorbed. Tests were performed using different NaOH concentrations (0.01–2 mol L^{-1}). The most $SO_4^{2-}$was desorbed (15 mg g^{-1}, 75% of the adsorbed SO_4^{2-}) when 2 mol L^{-1} NaOH was used. However, the adsorption capacity after the first regeneration process had been performed was <10 mg g^{-1}, and the adsorption capacity was almost 0 mg g^{-1} after five adsorption-desorption cycles. Strong alkaline conditions (i.e., a NaOH solution) would cause OH^- to readily attack the imino group and effectively desorb SO_4^{2-} [26] but excessively damage the PPy [27].

The OH^- concentration will be roughly the same in 12 mol L^{-1} NH_3·H_2O and 2 mol L^{-1} NaOH. SO_4^{2-} desorption over time using 12 mol L^{-1} NH_3·H_2O is shown in Figure 12(a). The percentage of the adsorbed SO_4^{2-} that was desorbed gradually increased over time and was ~30% at 5 min and >80% at 40 min. The desorption efficiency then remained stable. Regeneration tests were performed using 12 mol L^{-1} NH_3·H_2O at 288, 298, 308, and 318 K for 40 min. The desorption efficiency gradually decreased as the temperature increased (Figure 12(b)). The desorption efficiency was ~75% at 288 K but only ~30% at 318 K. This indicated that the desorption process was exothermic and that the desorption mechanism may have been spontaneous ion exchange involving OH^- released by NH_3·H_2O reacting with the imino groups in PPy to desorb SO_4^{2-}.

Adsorption-desorption recycling experiments using the PFB-GAC were performed using 12 mol L^{-1} NH_3·H_2O as the regenerant; the results are shown in Figure 13. The highest adsorption capacity and desorption efficiency

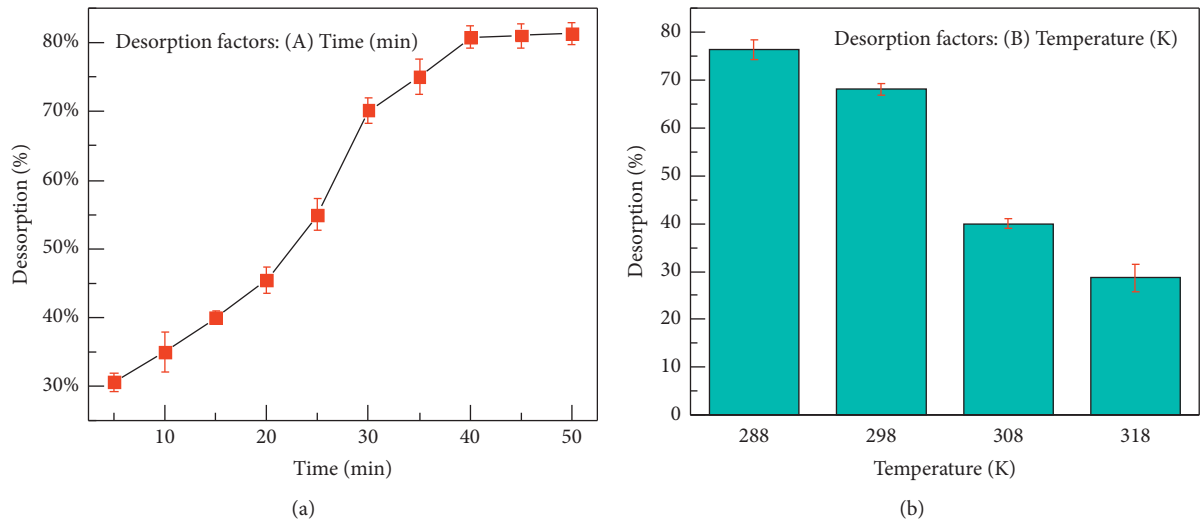

Figure 12: (a) Desorption efficiencies found using 12 mol L^{-1} ammonium hydroxide ($NH_3{\cdot}H_2O$) at different desorption periods. (b) Desorption efficiencies found using 12 mol L^{-1} $NH_3{\cdot}H_2O$ at different temperatures.

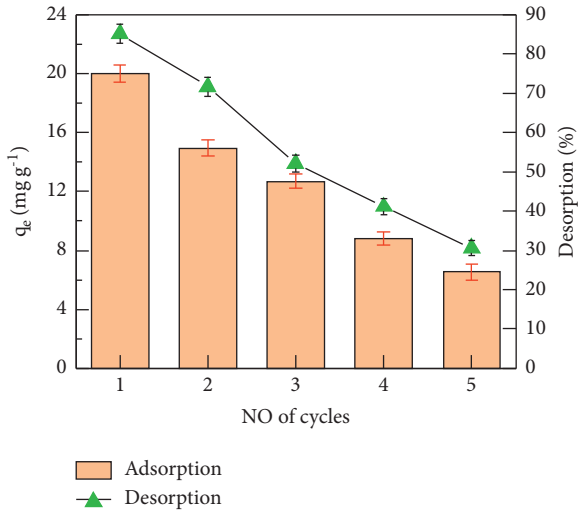

Figure 13: SO_4^{2-} adsorption and desorption data for five regeneration cycles using 12 mol L^{-1} $NH_3{\cdot}H_2O$ as the regenerant.

were found in the first cycle. The adsorption capacity was ~20 mg g^{-1}, and 12 mol L^{-1} $NH_3{\cdot}H_2O$ gave a desorption efficiency of 85% (i.e., higher than the 75% desorption efficiency found using 2 mol L^{-1} NaOH). Four more adsorption-desorption cycles were performed. The adsorption capacity gradually decreased as the number of regeneration cycles increased, and the desorption efficiency decreased (from 71.6% in cycle 2 to 30.5% in cycle 5). The adsorption capacity in cycle 5 was still >6 mg g^{-1} (in contrast, the PFB-GAC did not adsorb SO_4^{2-} after five regeneration cycles using NaOH). $NH_3{\cdot}H_2O$ is a weaker alkali than NaOH, so it damaged PPy less than NaOH. $NH_3{\cdot}H_2O$ is also a weak reducing agent, which would have been conducive to SO_4^{2-} desorption. The surface morphology of the PFB-GAC was not markedly altered by five regeneration cycles using $NH_3{\cdot}H_2O$ (Figure S7). The modified GAC doped with BSNa adsorbed and desorbed SO_4^{2-} well, possibly because the BSNa improved the alkali-resistance and stability of the modified GAC.

3.8. Analysis of the Mechanisms. No reduction of SO_4^{2-} was found to have occurred, because SO_4^{2-} is stable, and SO_4^{2-} removal mainly occurred through adsorption. The GAC removed little SO_4^{2-}, so it was concluded that only a small amount of physical adsorption to the GAC pore surfaces would have occurred when the modified GAC was used. The PFB on the PFB-GAC therefore mainly adsorbed SO_4^{2-}. The GAC acted as a carrier of the PFB. GAC has advantages over powdered activated carbon as a carrier, because less physical shedding of PFB will occur from GAC than from powdered activated carbon after multiple regeneration cycles, and the PFB-GAC particles would have had more regular shapes than would PFB-powdered activated carbon particles.

The PF-GAC and PFB-GAC clearly adsorbed SO_4^{2-} when the SO_4^{2-} concentration was low. This indicated that SO_4^{2-} was not removed from solution through a simple physical adsorption process. During the GAC modification process, Cl^- would have temporarily occupied the positively charged sites, which would have prevented strong removal of SO_4^{2-} through electrostatic attraction [22]. It was found in previous studies [8, 9] that SO_4^{2-} was removed by PPy-modified GAC mainly through ion exchange between Cl^- and SO_4^{2-}. The results of this experiment led to the same conclusion. During an adsorption test, the Cl^- concentration in solution gradually increased as the SO_4^{2-} concentration decreased, and the lower the Cl^- concentration, the poorer the adsorption effect. In summary, ion exchange played an important role in the adsorption of SO_4^{2-} by the PFB-GAC.

The mechanism involved in SO_4^{2-} removal by the PFB-GAC is shown in Figure 14. During the GAC doping and modification process, Py would have been oxidized by $FeCl_3{\cdot}(6H_2O)$, then polymerization of PPy would have occurred, and Cl^- would have been incorporated in the PPy. The Cl^- would have temporarily occupied the N^+ sites and

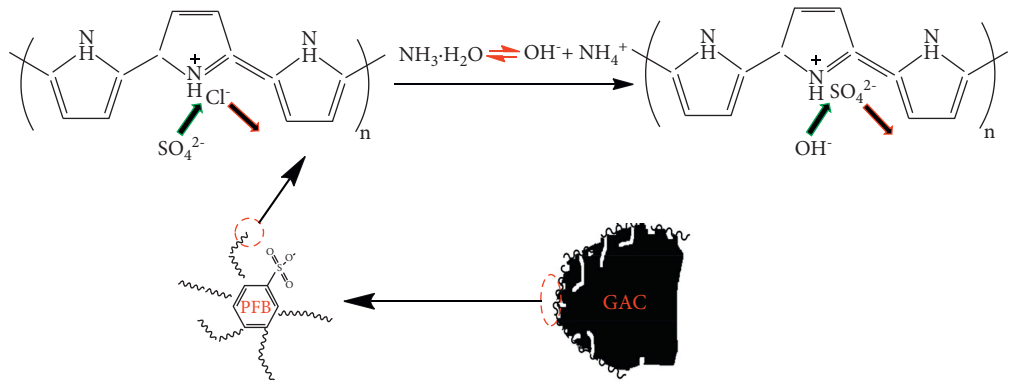

Figure 14: Mechanisms involved in producing the pyrrole-$FeCl_3$·($6H_2O$)-sodium benzenesulfonate-granular activated carbon and SO_4^{2-} adsorption.

would have been involved in SO_4^{2-} removal [22]. The SEM images (Figure 6) and EDS results (Figure 8) indicated that doping with BSNa made the PPy more planar than it would otherwise have been and limited three-dimensional growth of the PPy. The PPy would therefore have been securely anchored to the surfaces and voids of the GAC. This would have caused the N^+ content to be higher than it would have been in the absence of BSNa. It can be seen from the results of the PFB and PF experiments described in Section 3.2.1 that SO_4^{2-} was removed more effectively by the PFB-GAC than the PF-GAC. This indicated that doping the PPy with BSNa increased the number of ion exchange sites and improved SO_4^{2-} adsorption.

Strong acidic conditions will affect the surface charge of an adsorbent, the degree of ionization, and the adsorbent morphology [32]. Acidic conditions would have protonated the –NH groups in the PPy and increased the amount of SO_4^{2-} that became electrostatically adsorbed [38]. The positively charged sites in the PPy would have been attacked by OH^- under alkaline conditions, causing the PPy to be damaged [26].

Regenerating the PF-GAC using NH_3·H_2O allowed SO_4^{2-} adsorption and desorption to continue, because NH_3·H_2O will slowly release OH^- to desorb SO_4^{2-}. The SO_4^{2-} adsorption capacity after five adsorption-desorption cycles remained higher than the SO_4^{2-} adsorption capacity of the GAC.

4. Conclusions

Adsorption of SO_4^{2-} by the PFB-GAC was markedly improved by adding an appropriate amount of BSNa, and the PFB-GAC prepared using a P : F : B ratio of 1000 : 1500 : 1 had a higher SO_4^{2-} adsorption capacity than the PFB-GAC prepared using other P : F : B ratios. The SO_4^{2-} adsorption capacity of the PFB-GAC was 23.05 mg g^{-1} when the initial SO_4^{2-} concentration was 500 mg L^{-1}, the pH was 3, and the temperature was 298 K. Characterization and analysis of the PFB-GAC indicated that GAC doped with BSNa and loaded with PPy contained many N^+ sites and that ion exchange of Cl^- and SO_4^{2-} could occur. SO_4^{2-} adsorption by the PFB-GAC would mainly have occurred through ion exchange. The weak alkalinity of NH_3·H_2O made it a good agent for desorbing SO_4^{2-} from the PBF-GAC. The maximum SO_4^{2-} desorption efficiency for the PFB-GAC was 85%. The SO_4^{2-} adsorption capacity after five adsorption-desorption cycles was still higher than the SO_4^{2-} adsorption capacity of the GAC. The PFB-GAC is a new type of adsorbent that could be used to remove SO_4^{2-} from acidic wastewater.

Abbreviations

PPy: Polypyrrole
Py = P: Pyrrole
BSNa = B: Sodium benzenesulfonate
GAC: Granular activated carbon
PF-GAC: Pyrrole-$FeCl_3$·($6H_2O$)-granular activated carbon
PFB-GAC: Pyrrole-$FeCl_3$·($6H_2O$)-sodium benzenesulfonate-granular activated carbon.

Data Availability

All types of data used to support the findings of this study are available from the corresponding author upon request.

Conflicts of Interest

The authors declare that they have no conflicts of interest.

Acknowledgments

This work was supported by the Natural Science Foundation of Shanxi Province under grant 201801D121275 and the Key Research and Development (R&D) Projects of Shanxi Province under grant 201803D31050. The authors thank Gareth Thomas, PhD, from Liwen Bianji (Edanz) (https://www.liwenbianji.cn), for editing the language of a draft of this manuscript.

Supplementary Materials

Fig. S1. Adsorption of SO_4^{2-} by the GAC, FB-GAC, PF-GAC, and PB-GAC (GAC = granular activated carbon, FB-GAC = $FeCl_3$·($6H_2O$)-sodium benzenesulfonate-granular activated carbon, PF-GAC = pyrrole-$FeCl_3$·($6H_2O$)-granular

activated carbon, PB-GAC = pyrrole-sodium benzenesulfonate-granular activated carbon). *Fig. S2.* Pseudo-first-order kinetics plot of SO_4^{2-} adsorption to the PFB-GAC at different initial concentrations of SO_4^{2-} (PFB-GAC = pyrrole-$FeCl_3$·($6H_2O$)-sodium benzenesulfonate-granular activated carbon). *Fig. S3.* Pseudo-second-order kinetics plot of SO_4^{2-} adsorption to the PFB-GAC at different initial concentrations of SO_4^{2-} (PFB-GAC = pyrrole-$FeCl_3$·($6H_2O$)-sodium benzenesulfonate-granular activated carbon). *Fig. S4.* Langmuir isotherms for SO_4^{2-} adsorption to the PFB-GAC at different reaction temperature (PFB-GAC = pyrrole-$FeCl_3$·($6H_2O$)-sodium benzenesulfonate-granular activated carbon). *Fig. S5.* Freundlich isotherms for SO_4^{2-} adsorption to the PFB-GAC at different reaction temperature (PFB-GAC = pyrrole-$FeCl_3$·($6H_2O$sodium benzenesulfonate-granular activated carbon). *Fig. S6.* van 't Hoff plot used to determine thermodynamic parameters for SO_4^{2-} adsorption. *Fig. S7.* SEM image of PFB-GAC that had been regenerated five times using NH_3·H_2O at a magnification of 7000 (PFB-GAC = pyrrole-$FeCl_3$·($6H_2O$)-sodium benzenesulfonate-granular activated carbon). (*Supplementary Materials*)

References

[1] G. Cortecci, E. Dinelli, T. Boschetti, P. Arbizzani, L. Pompilio, and M. Mussi, "The Serchio River catchment, northern Tuscany: geochemistry of stream waters and sediments, and isotopic composition of dissolved sulfate," *Applied Geochemistry*, vol. 23, no. 6, pp. 1513–1543, 2008.

[2] W. D. Heizer, R. S. Sandler, E. Seal et al., "Intestinal effects of sulfate in drinking water on normal human subjects," *Digestive Diseases and Sciences*, vol. 42, no. 5, pp. 1055–1061, 1997.

[3] N. Wang, R. A. Dorman, C. D. Ivey et al., "Acute and chronic toxicity of sodium nitrate and sodium sulfate to several freshwater organisms in water-only exposures," *Environmental Toxicology and Chemistry*, vol. 39, no. 5, pp. 1071–1085, 2020.

[4] V. Iurchenko, E. Lebedeva, and E. Brigada, "Environmental safety of the sewage disposal by the sewerage pipelines," *Procedia Engineering*, vol. 134, pp. 181–186, 2016.

[5] H. Liu and Y. Frank Cheng, "Mechanism of microbiologically influenced corrosion of X52 pipeline steel in a wet soil containing sulfate-reduced bacteria," *Electrochimica Acta*, vol. 253, pp. 368–378, 2017.

[6] S. Tait, W. P. Clarke, J. Keller, and D. J. Batstone, "Removal of sulfate from high-strength wastewater by crystallisation," *Water Research*, vol. 43, no. 3, pp. 762–772, 2009.

[7] T. Raudsepp, M. Marandi, T. Tamm, V. Sammelselg, and J. Tamm, "Influence of ion-exchange on the electrochemical properties of polypyrrole films," *Electrochimica Acta*, vol. 122, pp. 79–86, 2014.

[8] P. Hou, T. Byrne, F. S. Cannon, B. P. Chaplin, S. Hong, and C. Nieto-Delgado, "Electrochemical regeneration of polypyrrole-tailored activated carbons that have removed sulfate," *Carbon*, vol. 79, pp. 46–57, 2014.

[9] S. Hong, F. S. Cannon, P. Hou, T. Byrne, and C. Nieto-Delgado, "Adsorptive removal of sulfate from acid mine drainage by polypyrrole modified activated carbons: effects of polypyrrole deposition protocols and activated carbon source," *Chemosphere*, vol. 184, pp. 429–437, 2017.

[10] Z. ALOthman, "A review: fundamental aspects of silicate mesoporous materials," *Materials*, vol. 5, no. 12, pp. 2874–2902, 2012.

[11] E.-R. Kenawy, A. A. Ghfar, S. M. Wabaidur et al., "Cetyltrimethylammonium bromide intercalated and branched polyhydroxystyrene functionalized montmorillonite clay to sequester cationic dyes," *Journal of Environmental Management*, vol. 219, pp. 285–293, 2018.

[12] Z. A. Alothman, A. H. Bahkali, M. A. Khiyami et al., "Low cost biosorbents from fungi for heavy metals removal from wastewater," *Separation Science and Technology*, vol. 55, no. 10, pp. 1766–1775, 2020.

[13] R. Parette and F. S. Cannon, "The removal of perchlorate from groundwater by activated carbon tailored with cationic surfactants," *Water Research*, vol. 39, no. 16, pp. 4020–4028, 2005.

[14] S. Kim, Y. Jang, M. Jang et al., "Versatile biomimetic conductive polypyrrole films doped with hyaluronic acid of different molecular weights," *Acta Biomaterialia*, vol. 80, pp. 258–268, 2018.

[15] R. V. Quevedo-Robles, G. A. Grijalva-Bustamante, T. del Castillo-Castro et al., "Novel electroconducting polypyrrole/carbon nanotube/alginate nanocomposites synthesized by hydrogen peroxide-mediated emulsion pathway," *Synthetic Metals*, vol. 253, pp. 100–109, 2019.

[16] R. Kumar, M. Oves, T. Almeelbi, N. H. Al-Makishah, and M. A. Barakat, "Hybrid chitosan/polyaniline-polypyrrole biomaterial for enhanced adsorption and antimicrobial activity," *Journal of Colloid and Interface Science*, vol. 490, pp. 488–496, 2017.

[17] J. Lippe and R. Holze, "Electrochemical in-situ conductivity and polaron concentration measurements at selected conducting polymers," *Synthetic Metals*, vol. 43, no. 1-2, pp. 2927–2930, 1991.

[18] A. Nautiyal, M. Qiao, J. E. Cook, X. Zhang, and T.-S. Huang, "High performance polypyrrole coating for corrosion protection and biocidal applications," *Applied Surface Science*, vol. 427, pp. 922–930, 2018.

[19] P. Qiao, B. Zhao, and Z. Nan, "Facile fabrication of ZnLa0.02Fe1.98O4/PPy and application in water treatment," *Materials Science and Engineering: B*, vol. 178, no. 20, pp. 1476–1482, 2013.

[20] S. Hong, S. Deng, X. Yao et al., "Bromate removal from water by polypyrrole tailored activated carbon," *Journal of Colloid and Interface Science*, vol. 467, pp. 10–16, 2016.

[21] M. J. García-Fernández, M. M. Pastor-Blas, F. Epron, and A. Sepúlveda-Escribano, "Proposed mechanisms for the removal of nitrate from water by platinum catalysts supported on polyaniline and polypyrrole," *Applied Catalysis B: Environmental*, vol. 225, pp. 162–171, 2018.

[22] J. J. Villora-Picó, M. Jesús García-Fernández, A. Sepúlveda-Escribano, and M. Mercedes Pastor-Blas, "Metal-free abatement of nitrate contaminant from water using a conducting polymer," *Chemical Engineering Journal*, vol. 403, Article ID 126228, 2021.

[23] M. Bhaumik, T. Y. Leswifi, A. Maity, V. V. Srinivasu, and M. S. Onyango, "Removal of fluoride from aqueous solution by polypyrrole/Fe3O4 magnetic nanocomposite," *Journal of Hazardous Materials*, vol. 186, no. 1, pp. 150–159, 2011.

[24] A. Nagaraj, D. Govindaraj, and M. Rajan, "Magnesium oxide entrapped Polypyrrole hybrid nanocomposite as an efficient selective scavenger for fluoride ion in drinking water," *Emergent Materials*, vol. 1, no. 1, pp. 25–33, 2018.

[25] S. Hong, F. S. Cannon, P. Hou, T. Byrne, and C. Nieto-Delgado, "Sulfate removal from acid mine drainage using polypyrrole-grafted granular activated carbon," *Carbon*, vol. 73, pp. 51–60, 2014.

[26] Z. Jin, K. Qi, Y. Qiu, Z. Chen, and X. Guo, "Degradation behavior of free-standing polypyrrole films in NaOH solution," *Polymer Degradation and Stability*, vol. 160, pp. 60–72, 2019.

[27] Z. Jin, Y. Qiu, Z. Chen, and X. Guo, "Effect of doping anions on the degradation of electrochemical activity of conductive polypyrrole in NaOH solution," *Corrosion Science*, vol. 138, pp. 252–265, 2018.

[28] T.-M. Wu, H.-L. Chang, and Y.-W. Lin, "Synthesis and characterization of conductive polypyrrole with improved conductivity and processability," *Polymer International*, vol. 58, no. 9, pp. 1065–1070, 2009.

[29] R. Li, Z. Xuefeng, W. Lixin, and Z. Fuqiang, "Conductivity and conducting mechanism of polypyrrole via chemical oxidative polymerization," *Journal of Semiconductors*, vol. 28, no. 9, pp. 1396–1401, 2007.

[30] A. H. Yuan, R. Li, and W. L. Xin, *Study on Chemical Oxidized Synthesis and Conductivity of Polypyrrole*, Journal of Yunnan University (Natural Sciences), Kunming, China, 2005.

[31] K. Qi, Y. Qiu, Z. Chen, and X. Guo, "Corrosion of conductive polypyrrole: effects of possibly formed galvanic cells," *Corrosion Science*, vol. 80, pp. 318–330, 2014.

[32] H. Pahlavanzadeh, R. Katal, and H. Mohammadi, "Synthesize of polypyrrole nanocomposite and its application for nitrate removal from aqueous solution," *Journal of Industrial and Engineering Chemistry*, vol. 18, no. 3, pp. 948–956, 2012.

[33] A. Mittal, M. Naushad, G. Sharma, Z. A. ALothman, S. M. Wabaidur, and M. Alam, "Fabrication of MWCNTs/ThO2 nanocomposite and its adsorption behavior for the removal of Pb(II) metal from aqueous medium," *Desalination and Water Treatment*, vol. 57, no. 46, pp. 21863–21869, 2016.

[34] H. Münstedt, "Properties of polypyrroles treated with base and acid," *Polymer*, vol. 27, no. 6, pp. 899–904, 1986.

[35] F. Beck and U. Barsch, "Corrosion of conducting polymers in aqueous electrolytes," *Synthetic Metals*, vol. 55, no. 2-3, pp. 1299–1304, 1993.

[36] M. Wang, G. Li, L. Huang et al., "Study of ciprofloxacin adsorption and regeneration of activated carbon prepared from Enteromorpha prolifera impregnated with H 3 PO 4 and sodium benzenesulfonate," *Ecotoxicology and environmental safety*, vol. 139, pp. 36–42, 2017.

[37] L. Fang, L. Zhao, X. Liang, H. Xiao, and L. Qian, "Effects of oxidant and dopants on the properties of cellulose/PPy conductive composite hydrogels," *Journal of Applied Polymer Science*, vol. 133, no. 34, pp. 43759–43764, 2016.

[38] W. Sun, W. Zhang, H. Li, Q. Su, P. Zhang, and L. Chen, "Insight into the synergistic effect on adsorption for Cr(vi) by a polypyrrole-based composite," *RSC Advances*, vol. 10, no. 15, pp. 8790–8799, 2020.

[39] I. M. Minisy, P. Bober, U. Acharya et al., "Cationic dyes as morphology-guiding agents for one-dimensional polypyrrole with improved conductivity," *Polymer*, vol. 174, pp. 11–17, 2019.